Frequency-Selective Rasorber Based on Square-Loop and Cross-Dipole Arrays

Yuping Shang, Zhongxiang Shen, *Senior Member*, *IEEE*, and Shaoqiu Xiao, *Member*, *IEEE*

***Abstract*—A novel design of a transmission window within the absorption band of a circuit analog absorber, named as frequency-selective rasorber (FSR), is presented. Based on an equivalent circuit model, the conditions are formulated to produce a passband with small insertion loss and to reduce the reflection at frequencies below and above the passband in the meanwhile. Simple design guidelines of our proposed FSR are then developed. With loaded lumped elements, the arrays of square-loop and cross-dipole are combined to realize its implementation. It is shown through measurements that an insertion loss of 0.68 dB can be obtained at 4.42 GHz and the fractional bandwidth for at least 10 dB reflection reduction within the lower and upper frequency bands is 92.3% under the normal incidence. A good agreement between simulated and measured results validates our design.**

***Index Terms*—Circuit analog absorber, frequency selective surface, radar absorber.**

I. Introduction

BANDPASS frequency selective surface (FSS) has found wide applications in many military communication systems due to its spatial filtering characteristics [1]. However, the bandpass FSS usually generates strong reflection at frequencies outside its passband. For the sake of improving the communication security and stealth performance of the platform on which the FSS is installed, design of bandpass FSS with reduced reflection from the rejection bands is attracting a growing attention. The radar absorber, which has been extensively investigated [2-5], lays the foundation for the reflection reduction of bandpass FSS. The resultant structures are radar absorbers with a transmission window, also called as frequency-selective rasorbers (FSR) [6].

In the past, such a structure was conceptually illustrated to reduce the out-of-band reflection from bandpass (slot-type) FSS [7]. The structure contains a lossy dielectric layer placed above the slot-type lossless FSS. The incident waves of frequencies outside the passband of the slot-type FSS can be absorbed similar to the operating principle of Salisbury screens, while retaining relatively undisturbed passband frequencies. In order to alleviate the transmission loss caused by the lossy layer, a resistive single-square-loop array [8, 9] and a resistor-loaded double-square-loop array [10] were recently used as the lossy layer placed above the slot-type lossless FSS with a dielectric spacer between them. At frequencies above the passband, the whole structure is similar to the circuit analog absorber so that its reflection reduction is obtained.

Furthermore, a resistive cross-dipole lossy layer placed above a metallic bandstop (strip-type) FSS was proposed in [11-13]. The reflection arising from the resonance of the strip-type lossless FSS could be reduced, while the passband was obtained at frequencies before the resonance of the lossless FSS. Similar designs using other unit cell patterns were also reported, such as the circular loop [14], double-square-loop [15], and skewed FSS lattice [16]. Two lossy layers were also placed above a strip-type lossless FSS with a dielectric spacer between different layers to realize the reflection reduction [17-19]. Structures composed of lossy layers and strip-type lossless FSS were also reported with an emphasis on the absorption band [20, 21], while no mention of the passband transmission was made.

For these reported rasorber designs, the passband is placed at a low-frequency away from the absorption band. Alternatively, only the reflection within the upper frequency band beyond the passband is usually reduced, whereas the strong reflection at the lower frequency band still remains, especially for the slot-type lossless FSS. In order to increase the design flexibility about the passband position relative to the absorption band and to reduce the reflection within both the lower and upper frequency bands, a novel rasorber design is proposed in this paper, based on the equivalent circuit analysis of rasorber with one lossy layer. Through the presented design, it is shown that a passband with a small insertion loss can be designed within the wide absorption band of a radar absorber. Meanwhile, the reflection at frequencies below and above the passband can be reduced, for both the strip-type and slot-type lossless FSSs.

II. Equivalent Circuit Analysis

Based on the reported rasorber designs, the side view of such structures consisting of one lossy layer placed above a lossless FSS is illustrated in Fig. 1 (a), which is adopted by our present design. In this paper, we focus on this simple rasorber with a dielectric spacer (thickness h_1 and relative permittivity ε_{r1}) between the lossy layer and lossless FSS. The equivalent circuit of the structure is described in Fig. 1 (b). It may be mentioned that the impedance Z_{F1} represents the lossy layer, while Z_{F2}

Manuscript received April X, 2014.

Y. Shang and S. Xiao are with the School of Physical Electronics, University of Electronic Science and Technology of China, Chengdu 610054, China (e-mail: shangyuping530@sina.com; xiaoshaoqiu@uestc.edu.cn).

Z. Shen is with the School of Electrical and Electronic Engineering, Nanyang Technological University, Singapore 639798 (e-mail: ezxshen@ntu.edu.sg).

This article has been accepted for publication in a future issue of this journal, but has not been fully edited. Content may change prior to final publication. Citation information: DOI 10.1109/TAP.2014.2357427, IEEE Transactions on Antennas and Propagation

denotes the lossless FSS. Z_0 and Z_1 are the characteristic impedances of free space and spacer, respectively.

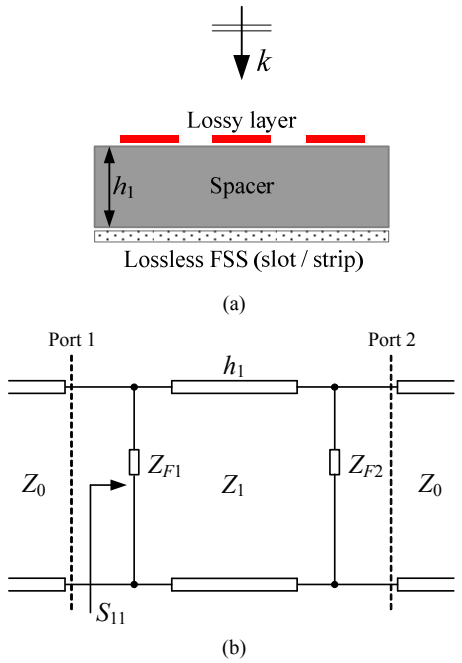

Fig. 1. (a) Side-view of reported rasorber designs with one lossy layer and (b) its equivalent circuit.

Since the primary goal of our rasorber is to introduce a passband within the absorption band, it is reasonable to set our design objective as follows. ($S_{11} = 0$, $S_{21} = 0$) at f_1 and f_3; ($S_{11} = 0$, $|S_{21}| = 1$) at f_2 on the condition that h_1 is a quarter-wavelength at f_2. S_{11} is the reflection coefficient from Port 1, while S_{21} is the transmission coefficient from Port 1 to Port 2. For frequencies between f_1 and f_3, it is desired that the reflection can be continuously less than a certain value (-10 dB is considered in our design). The relationship between three frequency points is $f_1 < f_2 < f_3$, which indicates that the passband is within the absorption band, thus the reflection reduction within the lower and upper frequency bands around the passband is satisfied.

According to the equivalent circuit described in Fig. 1 (b), the *ABCD* matrix of the network is written as,

$$\begin{bmatrix} A & B \\ C & D \end{bmatrix} = \begin{bmatrix} 1 & 0 \\ Y_{F1} & 1 \end{bmatrix} \begin{bmatrix} \cos\theta_1 & jZ_1 \sin\theta_1 \\ jY_1 \sin\theta_1 & \cos\theta_1 \end{bmatrix} \begin{bmatrix} 1 & 0 \\ Y_{F2} & 1 \end{bmatrix} \quad (1)$$

where $Y_{F1} = 1 / Z_{F1}$, $Y_1 = 1 / Z_1$, $Y_{F2} = 1 / Z_{F2}$, $\theta_1 = \beta_1 h_1 = 2\pi f h_1 \sqrt{\varepsilon_{r1}} / c$, f is the operating frequency and c is the speed of light in vacuum. Then using the conversion between *ABCD* matrix and [*S*] matrix [22], the expressions for S_{11} and S_{21} can be obtained,

$$S_{11} = \frac{j(\frac{Z_1}{Z_0} - \frac{Z_0}{Z_1})M - \frac{Z_0 N}{\tan\theta_1} + jZ_1(Z_{F1} - Z_0 - Z_{F2})}{j(\frac{Z_1}{Z_0} + \frac{Z_0}{Z_1})M + \frac{2M + Z_0 N}{\tan\theta_1} + jZ_1(Z_0 + N)} \quad (2a)$$

$$S_{21} = \frac{2Z_1 M}{(2M + Z_0 N)Z_1 \cos\theta_1 + [PM + Z_1^2(Z_0 + N)]j \sin\theta_1} \quad (2b)$$

where $M = Z_{F1}Z_{F2}$, $N = Z_{F1} + Z_{F2}$, $P = \frac{Z_1^2}{Z_0} + Z_0$.

As $S_{11} = 0$ at f_1 and f_3, which can be satisfied when the numerator of (2a) equals to zero, we obtain the following relationship between Z_{F1} and Z_{F2},

$$Z_{F1} = \frac{jZ_1Z_0 + (jZ_1 + \frac{Z_0}{\tan\theta_1})Z_{F2}}{jZ_1 - \frac{Z_0}{\tan\theta_1} + j(\frac{Z_1}{Z_0} - \frac{Z_0}{Z_1})Z_{F2}} \quad (3)$$

In addition, since $S_{21} = 0$ at f_1 and f_3, according to (2b), we obtain that $Z_{F1}Z_{F2} = 0$. Combining this with (3), a quadratic equation about Z_{F2} can be obtained,

$$(jZ_1 + \frac{Z_0}{\tan\theta_1})Z_{F2}^2 + jZ_1Z_0Z_{F2} = 0 \quad (4)$$

whose solutions are of the form

$$Z_{F2} = 0, \ \frac{-Z_1Z_0(Z_1 + \frac{jZ_0}{\tan\theta_1})}{Z_1^2 + \frac{Z_0^2}{\tan^2\theta_1}}. \quad (5)$$

It is obvious that the second solution of Z_{F2} is a complex number while its real part is negative. Without considering the negative resistance in this paper, we take zero as the solution of Z_{F2} at f_1 and f_3. Substituting $Z_{F2} = 0$ into (3) with the assumption that $\tan\theta_1 \neq 0$, we can obtain

$$Z_{F1} = \frac{Z_1Z_0(Z_1 - \frac{jZ_0}{\tan\theta_1})}{Z_1^2 + \frac{Z_0^2}{\tan^2\theta_1}} \overset{If\ Z_1 = Z_0}{=\!=\!=} \frac{Z_0(1 - \frac{j}{\tan\theta_1})}{1 + \frac{1}{\tan^2\theta_1}} \quad (6)$$

Thus, the required Z_{F1} and Z_{F2} for $S_{11} = 0$ and $S_{21} = 0$ at frequency points f_1 and f_3 are obtained. Due to the frequency dependence of θ_1, the values of Z_{F1} at f_1 and f_3 are not necessarily the same.

As both Z_{F1} and Z_{F2} in Fig. 1 are also complex impedances, they can be expressed in the form of $Z_{F1} = R_{F1} + jX_{F1}$, $Z_{F2} = jX_{F2}$. It should be noted that R_{F1}, X_{F1} and X_{F2} are all frequency dependent. At f_2, since $S_{11} = 0$ and $|S_{21}| = 1$, it is obvious that $|S_{21}| = 1$ can not be satisfied unless R_{F1} in Z_{F1} is zero at f_2, because of the dissipation property of the resistance. Thus a series $L_{sc}C_{sc}$ circuit is proposed to be connected in parallel with R_{F1}. L_{sc} and C_{sc} in the circuit model can be realized by lumped inductor and capacitor, respectively. In such case Z_{F1} is given

$$Z_{F1} = \frac{R_{F1}Q(Q + jR_{F1})}{R_{F1}^2 + Q^2} + jX_{F1} = \mathrm{Re}^{eq}(Z_{F1}) + jX_{F1} \quad (7)$$

where $Q = \omega L_{sc} - \frac{1}{\omega C_{sc}}$, $\omega = 2\pi f$. $\mathrm{Re}^{eq}(Z_{F1})$ denotes the impedance of R_{F1} connected in parallel with a series $L_{sc}C_{sc}$ circuit. It may be mentioned that $\mathrm{Re}^{eq}(Z_{F1})$ is not the conventional real part of a complex impedance, because an imaginary part is contained, as seen in (7). However, in such case we deem $\mathrm{Re}^{eq}(Z_{F1})$ as an equivalent real part of Z_{F1} for easy discussion.

The values of inductance L_{sc} and capacitance C_{sc} are so

This article has been accepted for publication in a future issue of this journal, but has not been fully edited. Content may change prior to final publication. Citation information: DOI 10.1109/TAP.2014.2357427, IEEE Transactions on Antennas and Propagation

chosen that the series connection of $L_{sc}C_{sc}$ resonates at f_2. It is seen from (7) that $\mathrm{Re}^{eq}(Z_{F1}) = 0$ at f_2. Then only the imaginary part of Z_{F1} is left at f_2, i.e., $Z_{F1} = jX_{F1}$. In comparison with $Z_{F1} = R_{F1} + jX_{F1}$, that is equivalent to the fact that R_{F1} is short-circuited at f_2 since the impedance of the $L_{sc}C_{sc}$ series combination at resonance is zero. As a simple instance, the impedance of a 300 Ω resistor connected in parallel with a series $L_{sc}C_{sc}$ circuit is shown in Fig. 2. The series $L_{sc}C_{sc}$ resonates at 4.95 GHz and it is seen that both the real and imaginary parts of the impedance are equal to zero at the resonance. Around the resonant frequency, the real part gradually rises up to the resistance value of 300 Ω, while the imaginary part introduced by the $L_{sc}C_{sc}$ connection turns from capacitive reactance before the resonance to inductive reactance after the resonance. It is also noticed that the relatively large L_{sc} and small C_{sc} values can help the real part return more quickly to 300 Ω with a smaller imaginary part at frequencies off the resonance.

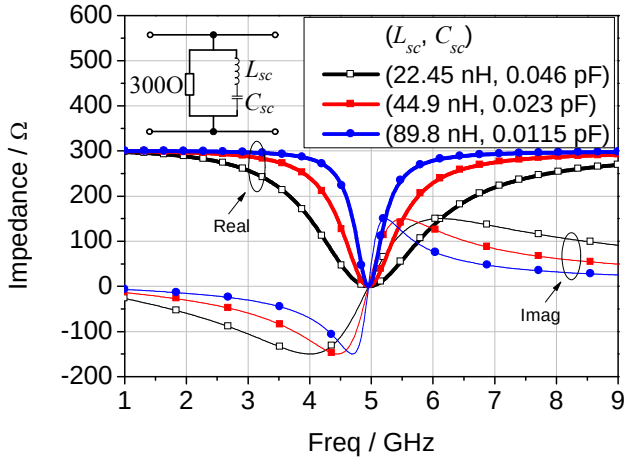

Fig. 2. The real and imaginary parts of a 300 Ω resistance connected in parallel with a series LC circuit. The impedance is calculated for different L_{sc} and C_{sc} values while their series resonance frequencies are kept the same.

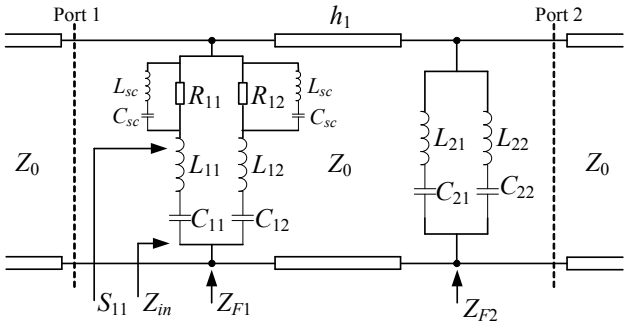

Fig. 3. Equivalent circuit model of the proposed rasorber.

In addition, it is seen from Fig. 1 that Z_{F1} and Z_{F2} are cascaded through a dielectric spacer with the thickness defined as a quarter-wavelength at f_2. Therefore, it can be inferred that if $Z_{F1} = jX_{F1}$ and $Z_{F2} = jX_{F2}$ can generate two parallel resonances at f_2, as the parallel resonance corresponds to a bandpass response, a passband at f_2 can then be obtained for our rasorber by these two cascaded lossless bandpass surfaces. Under this circumstance, (2a) and (2b) become

$$S_{11} = \frac{Z_1^2 - Z_0^2}{Z_1^2 + Z_0^2}, \tag{8a}$$

$$S_{21} = \frac{-j2Z_1Z_0}{Z_1^2 + Z_0^2}. \tag{8b}$$

It is seen that $S_{11} = 0$ requires $Z_1 = \pm Z_0$, while $|S_{21}| = 1$ also produces $Z_1 = \pm Z_0$. Thus the impedance of the spacer Z_1 should be selected as Z_0, which means that an air spacer should be used to obtain $|S_{21}| = 1$ and $S_{11} = 0$. That is understandable from the point view of impedance matching in transmission line circuits.

Based on the above observations, it is concluded for our design objectives,

(i) $Z_1 = Z_0$ (using air as the spacer thus $\varepsilon_{r1} = 1$);

(ii) $Z_{F2} = 0$ (lossless metallic FSS and series resonance) at f_1 and f_3, while the optimum values of Z_{F1} at f_1 and f_3 are expressed by (6);

(iii) The series connection of $L_{sc}C_{sc}$ resonates at f_2 and is connected in parallel with R_{F1}, while jX_{F1} and jX_{F2} produce a parallel resonance at f_2.

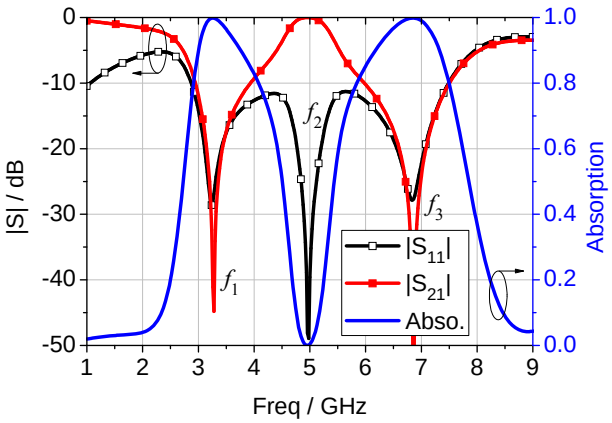

Fig. 4. Reflection, transmission and absorption of the rasorber calculated from the equivalent circuit model.

A specific circuit model that can fulfill those conditions for the proposed rasorber is shown in Fig. 3. The series connection of $L_{21}C_{21}$ in Z_{F2} is designed to resonate at f_1, while the series connection of $L_{22}C_{22}$ is intended to resonate at f_3, thus $Z_{F2} = 0$ is obtained at f_1 and f_3 because Z_{F2} consists of these two series LC circuits connected in parallel. The values of L_{21}, C_{21}, L_{22} and C_{22} can be determined from the physical dimensions of the involved FSS structures [23, 24]. In addition, a parallel resonance can be established at a frequency between these two series connections of Z_{F2} at f_1 and f_3 [25], which produces a passband at f_2. In the meanwhile, $L_{sc}C_{sc}$ in Z_{F1} resonates at f_2, making resistances R_{11} and R_{12} short-circuited, and resulting in a passband between the series resonances of $L_{11}C_{11}$ and $L_{12}C_{12}$. The pass bands of Z_{F2} and Z_{F1} should be at the same frequency to obtain a good transmission or small insertion loss. As a simple start of obtaining a passband at f_2 for the rasorber, the inductances and capacitances in Z_{F1} can be selected to be $L_{11} = L_{21}$, $C_{11} = C_{21}$, $L_{12} = L_{22}$, $C_{12} = C_{22}$ as an initial guess. The values

This article has been accepted for publication in a future issue of this journal, but has not been fully edited. Content may change prior to final publication. Citation information: DOI 10.1109/TAP.2014.2357427, IEEE Transactions on Antennas and Propagation

of resistances R_{11} and R_{12} are determined for desirable frequency responses of reflection through quick circuit simulation.

Simulated reflection and transmission coefficients for the circuit model are shown in Fig. 4. Based on the calculated equivalent inductances and capacitances of FSS structures, the circuit simulation is conducted with the following optimized values: L_{11} = 34.6 nH, C_{11} = 0.062 pF, R_{11} = 350 Ω, L_{12} = 16 nH, C_{12} = 0.03 pF, R_{12} = 440 Ω, L_{sc} = 44.9 nH, C_{sc} = 0.023 pF, h_1 = 14.6 mm, L_{21} = 18.2 nH, C_{21} = 0.13 pF, L_{22} = 11.22 nH, C_{22} = 0.048 pF. It is seen that a passband is obtained with an insertion loss of 0.0003 dB around 4.95 GHz. The reflection and transmission are -26.9 dB and -44.8 dB at 3.28 GHz, respectively. At 6.86 GHz the reflection and transmission are -27.7 dB and -61.9 dB, respectively. The absorption of the rasorber calculated as $(1 - |S_{11}|^2 - |S_{21}|^2)$ is also presented in Fig. 4. High absorption occurs around f_1 and f_3 so that a small $|S_{11}|$ can be obtained, while the absorption at f_2 is close to zero so as to ensure a good transmission. It may be mentioned that the backward transmission coefficient S_{12} exactly equals to $|S_{21}|$ due to the reciprocity of the network. The circuit simulation is conducted mainly to demonstrate that a transmission window with a small insertion loss can be introduced within an absorption band by the proposed rasorber.

In terms of the passband bandwidth, the relatively small L_{sc} and large C_{sc} are helpful to widen the bandwidth. However, the absorption at frequencies other than the passband demands a relatively large L_{sc} and small C_{sc}, as indicated in Fig. 2. Thus it can be pointed out that the passband bandwidth of the rasorber is mainly limited by the value of $L_{sc}C_{sc}$ once L_{ij} and C_{ij} (i = 1, 2; j = 1, 2) are determined. Moreover, once Z_{F2} is determined, the absorption bandwidth is generally bounded by the realizable Z_{F1}, although the optimum Z_{F1} is given by (3).

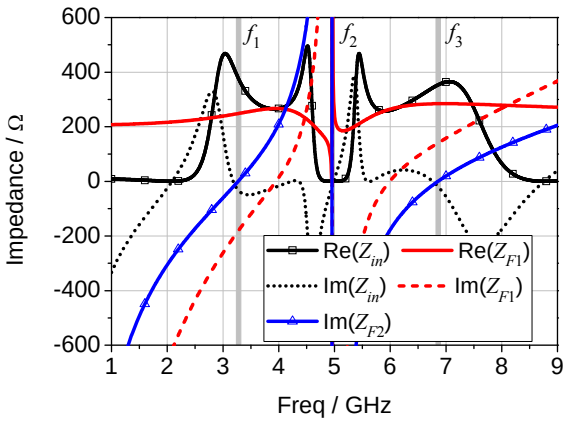

Fig. 5. Real and imaginary parts of Z_{in}, Z_{F1} and Z_{F2} of the rasorber obtained from the equivalent circuit model.

The real and imaginary parts of Z_{in}, Z_{F1} and Z_{F2} shown in Fig. 5 further verify our rasorber analysis. Z_{F2} equals to zero at f_1 and f_3. Z_{F1} from the circuit model at f_1 and f_3 are, respectively, 248.6 $-j180$ Ω and 284.4 $+j141.1$ Ω, which are quite close to the 268 $-j170.9$ Ω and 281.7 $+j163.9$ Ω calculated from (6) at f_1 and f_3, respectively. At f_2, both Z_{F2} and Z_{F1} are parallel resonances, and the real part of Z_{F1} nearly equals to zero, which ensures that the maximum transmission can be realized. The imaginary part of Z_{in} shows the resonances of the whole circuit, while its real part displays the impedance matching with Z_0 around the resonance.

III. Implementation of the Rasorber

The series connections of LC in Z_{F2} indicate that strip-type lossless FSS should be used to realize Z_{F2}. In the design described in this paper, the thickness and relative permittivity of the substrate used to support the metallic strips are 0.508 mm and 2.2, respectively. The square-loop array and cross-dipole array are combined to realize the required circuit parameters and implement the rasorber with dual-polarization functionality, their equivalent circuit parameters under the normal incidence can be determined from their physical dimensions [23, 24]. The lossless square-loop array is responsible for $L_{21}C_{21}$, while the lossless cross-dipole array is for $L_{22}C_{22}$ in Z_{F2}. ANSYS high frequency structure simulator (HFSS) is employed to evaluate the rasorber performance.

Based on the equivalent circuit model and the analysis conducted, we can have the following design guidelines so that a rasorber with a transmission window in the absorption band can be quickly designed.

(1) Once the passband frequency f_2 is specified, the thickness of the air spacer $h_1 \approx \lambda_2/4$ is then determined. Moreover, the passband frequency of Z_{F2} which is expressed as $\frac{1}{2\pi}\sqrt{\frac{C_{21}+C_{22}}{C_{21}C_{22}(L_{21}+L_{22})}}$ [25] should be equal to f_2; $L_{sc}C_{sc}$ should be selected such that $(2\pi\sqrt{L_{sc}C_{sc}})^{-1} = f_2$.

(2) The associated stopband frequencies f_1 and f_3 where reflection is to be reduced are obtained with $(2\pi\sqrt{L_{21}C_{21}})^{-1} = f_1$ and $(2\pi\sqrt{L_{22}C_{22}})^{-1} = f_3$. As aforementioned, L_{11}, C_{11}, L_{12} and C_{12} can be the same as L_{21}, C_{21}, L_{22} and C_{22} for the initial estimation.

(3) Once f_1 and f_3 are obtained, the optimum values of Z_{F1} for zero reflection at f_1 and f_3 can be computed. In combination with R_{11} and R_{12}, which are closely related to the absorption, the desirable frequency responses of the rasorber can be obtained through a quick circuit simulation. It may be mentioned that a relatively large inductance is preferred for the LC series connections in Z_{F1} on the condition that their resonance frequencies are unchanged.

(4) In terms of circuit parameters, formulae in [23, 24] are used to obtain an initial estimate of the physical dimensions of the square-loop and cross-dipole.

(5) With the estimated dimensions, the full-wave simulator HFSS may be used to fine-tune the structure. A thin substrate with low relative permittivity should be selected to facilitate the fabrication.

More specifically, as the passband of our rasorber is f_2 = 4.95 GHz, we obtain h_1 = 15.2 mm as an estimate. From the circuit model, the LC parameters in the circuit model can be adjusted in terms of f_2, f_1 and f_3. It can be seen from the guidelines that f_1 and f_3 are mainly determined by the square-loop and cross-dipole arrays, respectively, while f_2 is co-determined by

This article has been accepted for publication in a future issue of this journal, but has not been fully edited. Content may change prior to final publication. Citation information: DOI 10.1109/TAP.2014.2357427, IEEE Transactions on Antennas and Propagation

those two arrays. This implies that these three frequencies are thus related to one another.

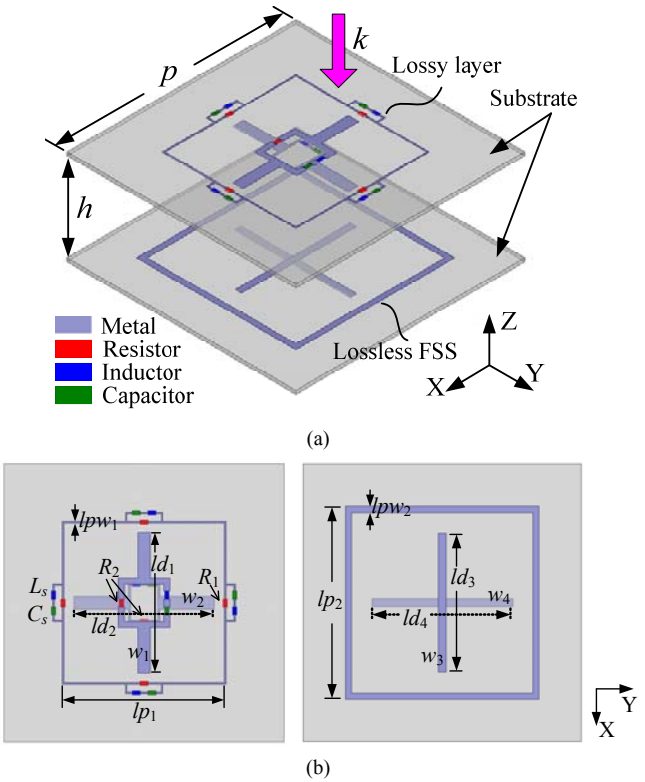

Fig. 6. (a) Perspective view of the unit cell structure of the proposed rasorber. (b) Top view of the lossy layer and lossless FSS unit cells.

A. Preliminary Design

Fig. 6 illustrates the unit cell geometry of the rasorber. There are one square-loop and one cross-dipole in each unit cell of the lossless FSS (Z_{F2}), while lumped resistors are inserted in each edge of the square-loop and each strip of the cross-dipole for the lossy layer (Z_{F1}). Moreover, a series connection of lumped inductor and capacitor is connected in parallel with each lumped resistor. It may be mentioned that the parasite effect of these lumped inductor and capacitor may be taken into account at high frequencies in the full-wave model. In order to facilitate soldering the lumped elements and to avoid cross-over, the strip of the cross-dipole along the x-axis is printed on the top-layer of the thin substrate, while the strip along the y-axis is on the bottom-layer. The dimensions are: $lp_1 = 21$ mm, $lpw_1 = 0.2$ mm, $R_1 = 50\ \Omega$, $L_s = 1.5$ nH, $C_s = 0.2$ pF, $ld_1 = 18.2$ mm, $w_1 = 1.6$ mm, $R_2 = 330\ \Omega$, $ld_2 = 18$ mm, $w_2 = 1.6$ mm, $p = 36$ mm, $h = 14$ mm, $lp_2 = 25$ mm, $lpw_2 = 0.8$ mm, $ld_3 = 18$ mm, $w_3 = 1$ mm, $ld_4 = 18.2$ mm, $w_4 = 1$ mm.

In Fig. 6, it is seen that the x-z plane is the plane of incidence. Thus the incident wave with its electric field directed along the y-axis is TE polarization, while the incidence of TM polarized wave has its magnetic field along the y-axis. By virtue of master and slave boundaries as well as Floquet ports in HFSS, the simulated reflection and transmission coefficients of the lossless FSS are shown in Fig. 7 (a). The slight structure difference of the dipole strips along the y-axis and x-axis accounts for the slightly different frequency responses under the normal incidence of TE and TM polarizations. The two transmission zeros around 3.22 GHz and 6.95 GHz corresponds to the series resonances, while the transmission pole around 5.1 GHz corresponds to the parallel resonance.

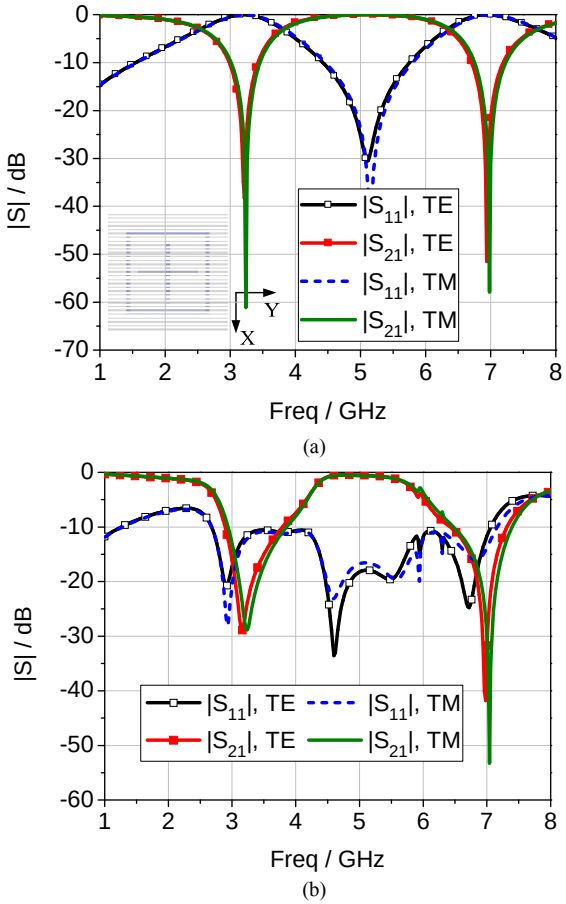

Fig. 7. Reflection and transmission of (a) the lossless FSS and (b) the rasorber obtained from HFSS using periodic boundaries under the normal incidence.

Fig. 7 (b) shows the simulated reflection and transmission of the rasorber. It is seen that the insertion loss for TE polarization is 0.44 dB at 4.76 GHz and 0.54 dB at the same frequency for TM polarization. The actual values of Z_{F1} realized by square-loop and cross-dipole arrays loaded with lumped elements may be different from the optimized value, which may account for the slight shift between $|S_{11}|$ and $|S_{21}|$ minima around f_1 and f_3. It may be pointed out that these minima around either f_1 or f_3 can be co-located through properly designing the geometries. The frequency shift between circuit and HFSS simulation results may be attributed to the difference in Z_{F1} value, the interaction of arrays and thin substrate, which are not considered in the circuit model for the sake of analysis simplicity. The small ripple around 6 GHz results from the harmonic resonances of lossy and lossless square-loop arrays whose fundamental resonances are around f_1. Compared with the lossless FSS, the reflection from the rasorber is reduced to below -10 dB with a fractional bandwidth of 91.3% from 2.67 GHz to 7.16 GHz, while the transmission band is retained. However, the large periodicity of this design may cause a degraded performance when the oblique incidence of a plane

This article has been accepted for publication in a future issue of this journal, but has not been fully edited. Content may change prior to final publication. Citation information: DOI 10.1109/TAP.2014.2357427, IEEE Transactions on Antennas and Propagation

wave is considered. Next section will introduce a miniaturized design that exhibits a relatively stable angular response.

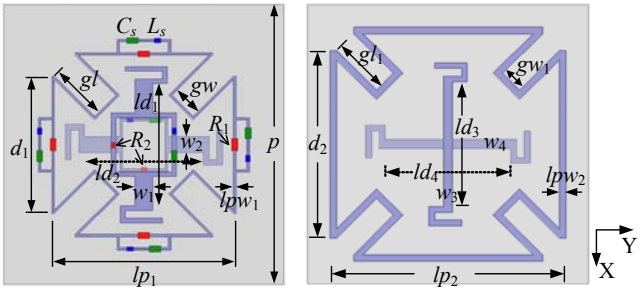

Fig. 8. Top view of the lossy layer and lossless FSS unit cells of the rasorber with reduced cell size.

B. Miniaturized Design

In order to reduce the periodicity or unit cell size of the structure to stabilize the angular response, folded strips are introduced at the four corners of each square-loop and the two ends of each dipole, as shown in Fig. 8. The dimensions are: lp_1 = 16.4 mm, lpw_1 = 0.2 mm, d_1 = 12.2 mm, gl = 5.1 mm, gw = 2.69 mm, R_1 = 50 Ω, L_s = 1.5 nH, C_s = 0.2 pF, ld_1 = 10.9 mm, w_1 = 1.6 mm, ld_2 = 10.6 mm, w_2 = 1.4 mm, R_2 = 330 Ω, p = 25 mm, h = 12 mm, lp_2 = 21 mm, lpw_2 = 0.6 mm, d_2 = 16.8 mm, gl_1 = 5 mm, gw_1 = 2.12 mm, ld_3 = 11.2 mm, w_3 = 0.8 mm, ld_4 = 11.2 mm, w_4 = 0.8 mm.

Under the normal incidence shown in Fig. 9, the insertion loss for TE polarization is 0.34 dB at 4.64 GHz and for TM polarization is 0.77 dB at 4.56 GHz. The bandwidth for reflection less than -10 dB is 88.9% from 2.75 GHz to 7.15 GHz for TE polarization and 92.6% from 2.76 GHz to 7.52 GHz for TM polarization. The $|S_{11}|$ and $|S_{21}|$ minima around either f_1 or f_3 are almost co-located. The passband transmission hardly changes under different angles of incidence for both polarizations. It is also seen that the reflection under the oblique incidence of TE polarization is relatively stable up to θ = 30º, while the high-frequency response of reflection under the oblique incidence of TM polarization deteriorates due to the harmonic resonances of lossy and lossless square-loop arrays. Methods of improving the performance under the oblique incidence may include the use of dielectric matching slab [26] and the optimization of the unit cell structure for intended oblique angle of incidence. For the array resonant at f_1, it is suggested to adopt a unit cell structure with its harmonic resonance located outside the upper frequency end of the rasorber. Thus the degradation caused under the oblique incidence can be alleviated over the frequency band of interest.

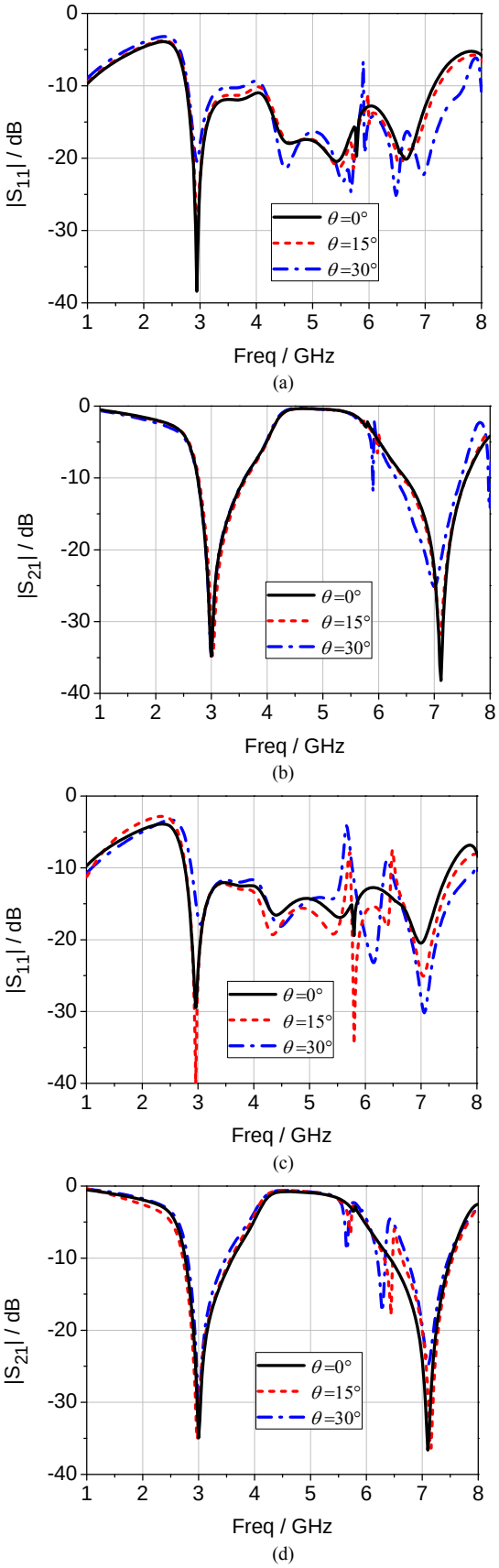

Fig. 9. Simulated results of the rasorber with reduced cell size under different angles of incidence: (a) reflection and (b) transmission under TE polarization; (c) reflection and (d) transmission under TM polarization.

This article has been accepted for publication in a future issue of this journal, but has not been fully edited. Content may change prior to final publication. Citation information: DOI 10.1109/TAP.2014.2357427, IEEE Transactions on Antennas and Propagation

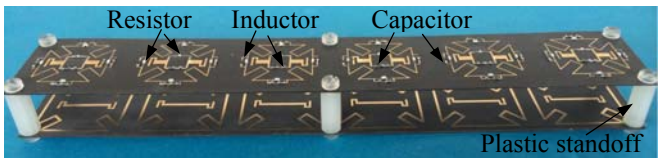

Fig. 10. Photo of the fabricated 1 × 6 rasorber with strip-type lossless FSS.

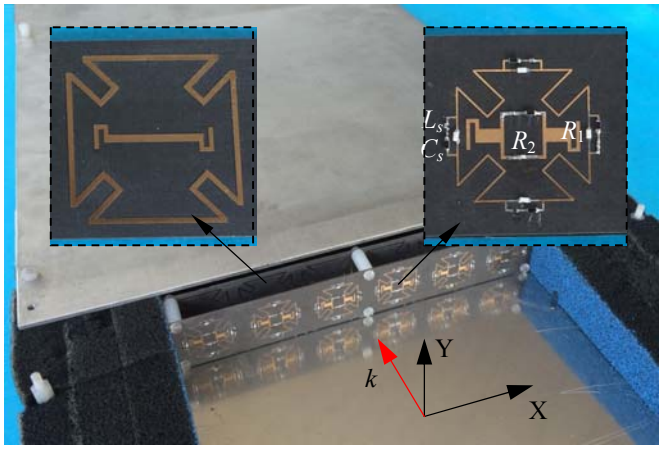

Fig. 11. Photo of the test setup.

IV. Experimental Measurements and Discussions

A. Experimental Measurements

In order to verify the simulations, the rasorber design in Fig. 8 is fabricated and measured. A photo of the fabricated prototype consisting of six cells in one direction on RT/duroid 5880 substrate is shown in Fig. 10. The wideband parallel-plate waveguide structure described in [27] is used to measure the reflection and transmission coefficients of the one-dimensional array of the rasorber. A photo of the test setup is provided in Fig. 11. The measured reflection and transmission of the prototype under the normal incidence of TE polarization are shown in Fig. 12. The measured insertion loss is 0.68 dB at 4.42 GHz and the bandwidth for reflection less than -10 dB is 92.3% from about 2.5 GHz to 6.79 GHz. The frequency shift, occurring for the reflection and maximum transmission frequency point, may be attributed to the increase in actual values of lumped capacitors and inductors as the frequency approaches their self-resonant frequencies, the uncertainty in resistance value of surface mount resistors as well as the fabrication tolerance. In spite of this, it is seen that the behavior is generally comparable. The relatively good agreement between simulated and measured results verifies the validity of our analysis.

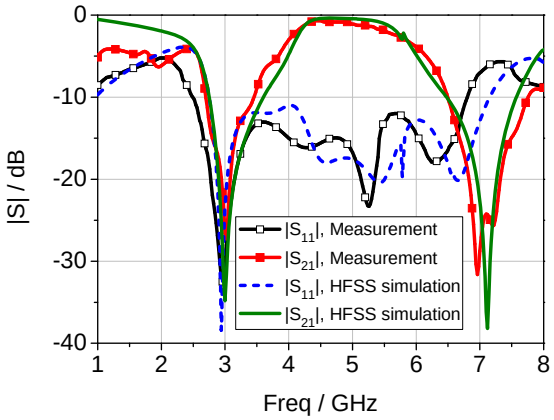

Fig. 12. Measured and simulated reflection and transmission of the rasorber under the normal incidence of TE polarization.

B. Discussions

Through connecting a series *LC* circuit in parallel with the resistive component in the lossy layer, it is seen from the equivalent circuit analysis that the resistance of Z_{F1} can be short-circuited at the selected passband. Thus the dissipation of incident energy becomes frequency-selective. In most radome applications, the antenna operating within the rasorber's passband can reside under the lossless FSS for transmitting or receiving friendly electromagnetic signals, while the lossy layer faces the incoming radar threats. For the sake of completeness, the frequency-selective lossy layer placed above a traditional slot-type lossless FSS is also studied.

Since a simple slot-type FSS usually associates with the bandpass response that can be described as a parallel *LC* circuit, neither solution in (5) can be satisfied at f_1 and f_3 when Z_{F2} in Fig. 3 is a parallel *LC* circuit. Thus S_{21} at f_1 and f_3 can not theoretically be equal to zero. The optimum values of Z_{F1} for $S_{11} = 0$ at f_1 and f_3 are expressed by (3). The resonant frequency of the slot-type FSS should be designed to be the same as the passband frequency of Z_{F1}.

As an example, a design using a simple square-slot array as the lossless FSS is shown in Fig. 13. The lossy layer is also implemented with folded square-loop and cross-dipole arrays. The dimensions are: $lp_1 = 15.8$ mm, $lpw_1 = 0.2$ mm, $d_1 = 12$ mm, $gl = 4.8$ mm, $gw = 2.4$ mm, $R_1 = 50\ \Omega$, $L_s = 1.5$ nH, $C_s = 0.2$ pF, $ld_1 = 10.9$ mm, $w_1 = 1.8$ mm, $ld_2 = 10.6$ mm, $w_2 = 1.4$ mm, $R_2 = 330\ \Omega$, $p = 25$ mm, $h = 11$ mm, $sl = 16.7$ mm, $sw = 0.6$ mm. For the square-slot FSS in Fig. 13 (a), the reflection can be reduced to below -10 dB with a bandwidth of 100% from 2.83 GHz to 8.51 GHz for TE polarization, while 98.2% from 2.85 GHz to 8.35 GHz for TM polarization. The transmission band is retained with the insertion loss of 0.36 dB and 0.74 dB at 4.66 GHz for TE and TM polarizations, respectively.

This article has been accepted for publication in a future issue of this journal, but has not been fully edited. Content may change prior to final publication. Citation information: DOI 10.1109/TAP.2014.2357427, IEEE Transactions on Antennas and Propagation

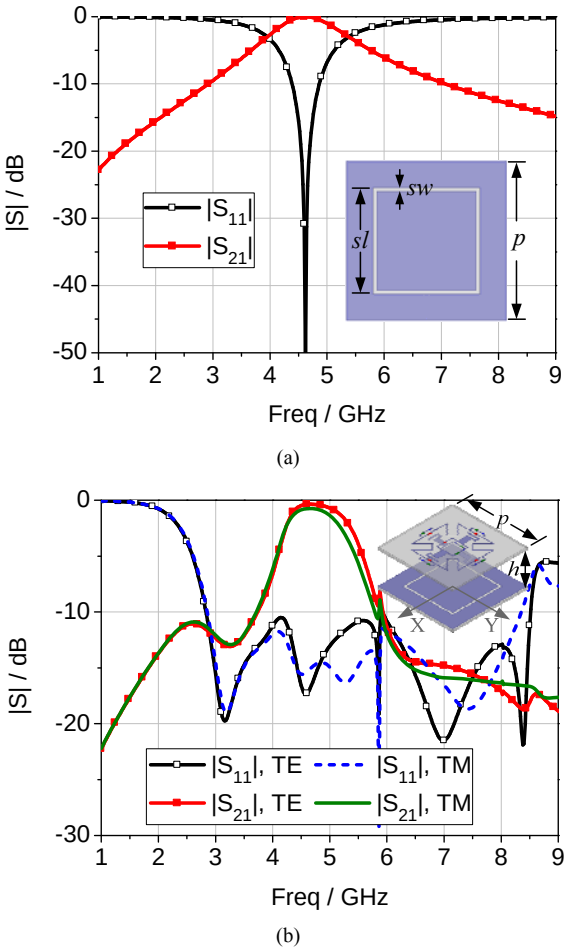

Fig. 13. Simulated reflection and transmission of (a) the square-slot lossless FSS and (b) the lossy layer placed above the square-slot FSS under the normal incidence.

TABLE I
TRANSMISSION AND REFLECTION COMPARISON

Ref.	Maximum transmission and f_T	FBW, f_L	Thickness (unit: λ_L)	Number of lossy layer	Lossless FSS type
[8]	-0.3dB, 4.6GHz	57.2%, 10GHz	0.167	1	slot
[10]	Mea. -1dB, 1GHz	Mea. 100%, 3GHz	0.105	1	slot
[11]	-0.1dB, 0.9GHz; -0.9dB, 1.8/1.9GHz	Mea. -10dB reflection around 5.37GHz	0.222	1	strip
[19]	-1.9dB, 1GHz	100% (-19dB reflection), 5.3GHz	0.131	2	strip
Our work	Mea. -0.68dB, 4.42GHz	Mea. 92.3%, 2.5GHz	0.108	1	strip
	-0.36dB, 4.66GHz	100%, 2.83GHz	0.113	1	slot

FBW = fractional bandwidth of -10 dB reflection, f_L = lowest frequency of -10 dB reflection, λ_L = free space wavelength at f_L, Mea. = measurement.

In order to better understand the performance of our presented rasorber against reported designs, we list the passband maximum transmission and its frequency f_T, the absorption bandwidth and lowest frequency of 10 dB absorption band as well as the structure thickness in Table I. It may be mentioned that only the performance under TE polarization is listed in the table for the designs in [19] and our work. Through the relative relationship between f_T and f_L, it is seen that the passband of all the previously reported designs is uniformly below their absorption band and only the reflection within the upper frequency band beyond the passband is reduced, whereas the passband of our proposed rasorber is within the absorption band and thus the reflection reduction can be realized at both sides of the passband. Moreover, the passband transmission performance can be properly retained. The fractional bandwidth of reflection reduction is larger than or comparable to those reported designs employing one lossy layer and the total thickness of our design is relatively small.

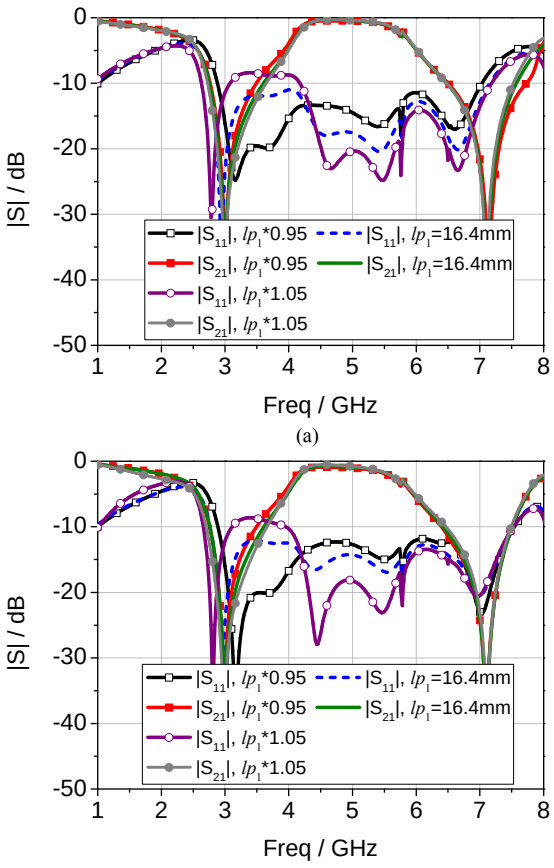

Fig. 14. The effect of lp_1 on the rasorber performance under the normal incidence of (a) TE and (b) TM polarizations.

With the aim of determining the sensitivity of the rasorber performance to the variation of geometrical and element parameters, the rasorber parameters in Fig. 8 are varied by 5% with respect to their optimized values. It is found that the passband transmission is almost unchanged under such variations; the parameters (lp_1, gl, ld_1, ld_2, p, h, lp_2, gl_1, ld_3, ld_4, C_s) obviously affect the frequency dependence of the reflection. However, only the variation in lp_1 significantly influences the fractional bandwidth of 10 dB reflection reduction. The 5%

This article has been accepted for publication in a future issue of this journal, but has not been fully edited. Content may change prior to final publication. Citation information: DOI 10.1109/TAP.2014.2357427, IEEE Transactions on Antennas and Propagation

increment of lp_1 makes part of the reflection coefficient within the lower frequency band larger than -10 dB. The effects of this variation are examined in Fig. 14. It may be concluded that our designed rasorber is not sensitive to parameter variations except the lp_1.

V. Conclusion

It has been shown that a passband can be introduced within the absorption band of a radar absorber. The transmission with a small insertion loss has been realized by connecting a series *LC* circuit in parallel with the resistive component in the lossy layer and properly designing the lossless FSS. Simple design guidelines have been developed for implementing the proposed frequency-selective rasorber. Compared with other reported designs, the reflection at both the lower and upper frequency bands around the passband can be reduced with the proposed rasorber, which can help to improve the communication security and low observability of military systems.

References

[1] B. A. Munk, *Frequency Selective Surfaces: Theory and Design*. NY: John Wiley & Sons, Inc., 2000.
[2] E. F. Knott, J. F. Shaeffer and M. T. Tuley, *Radar Cross Section*, 2nd ed. NC: SciTech Publishing, Inc., 2004.
[3] J. Sun, L. Liu, G. Dong, and J. Zhou, "An extremely broad band metamaterial absorber based on destructive interference," *Opt. Express*, vol. 19, no. 22, pp. 21155-21162, Oct. 2011.
[4] O. Luukkonen, F. Costa, C. R. Simovski, A. Monorchio, and S. A. Tretyakov, "A thin electromagnetic absorber for wide incidence angles and both polarizations," *IEEE Trans. Antennas Propag.*, vol. 57, no. 10, pp. 3119-3125, Oct. 2009.
[5] A. Fallahi, A. Yahaghi, H.-R. Benedickter, H. Abiri, M. Shahabadi, and C. Hafner, "Thin wideband radar absorber," *IEEE Trans. Antennas Propag.*, vol. 58, no. 12, pp. 4051-4058, Dec. 2010.
[6] B. A. Munk, *Metamaterials: critique and alternatives*. NY: John Wiley & Sons, Inc., 2009.
[7] W. S. Arceneaux, R. D. Akins and W. B. May, "Absorptive/transmissive radome," U.S. Patent 5 400 043, Mar. 1995.
[8] F. Costa and A. Monorchio, "A frequency selective radome with wideband absorbing properties," *IEEE Trans. Antennas Propag*., vol. 60, no. 6, pp. 2740-2747, Jun. 2012.
[9] F. Costa and A. Monorchio, "Absorptive frequency selective radome," 2011 *URSI General Assembly and Scientific Symp*., 2011.
[10] L.-G. Liu, Y.-Q. Li, Q.-Z. Meng, W.-W. Wu, J.-J. Mo, Y.-Q. Fu and N.-C. Yuan, "Design of an invisible radome by frequency selective surfaces loaded with lumped resistors," *Chin. Phys. Lett.*, vol. 30, no. 6, 2013.
[11] G. I. Kiani, A. R. Weily and K. P. Esselle, "A novel absorb/transmit FSS for secure indoor wireless networks with reduced multipath fading," *IEEE Microw. Wireless Compon. Lett*., vol. 16, no. 6, pp. 378-380, Jun. 2006.
[12] G. I. Kiani, A. R. Weily and K. P. Esselle, "Frequency selective surface absorber using resistive cross-dipoles," *IEEE Int. Symp. Antennas Propag. Soc*., 2006, pp. 4199-4202.
[13] G. I. Kiani, K. L. Ford, K. P. Esselle, A. R. Weily and C. J. Panagamuwa, "Oblique incidence performance of a novel frequency selective surface absorber," *IEEE Trans. Antennas Propag*., vol. 55, no. 10, pp. 2931-2934, Oct. 2007.
[14] U. Rafique, G. I. Kiani, M. M. Ahmed and S. Habib, "Frequency selective surface absorber for WLAN security," in *Proc. 5th Eur. Conf. Antennas Propag*., 2011, pp. 872-875.
[15] M. Abdin, U. Rafique, F. Malik, S. Qasim, M. A. Khan and M. M. Ahmed, "A novel dual-band frequency selective surface absorber," *Int. J. Electromagn. Applicat*., vol. 2, no. 6, pp. 182-185, 2012.
[16] U. Rafique, M. A. Khan, M. T. Afzal, F. Malik and S. Qasim, "Skewed frequency selective surface absorber," *Int. J. Advancements in Research and Tech*., vol. 1, no. 7, Dec. 2012.
[17] A. Motevasselian and B. L. G. Jonsson, "A partially transparent Jaumann absorber applied to an aircraft wing profile," *IEEE Int. Symp. Antennas Propag. Soc*., 2010.
[18] A. Motevasselian and B. L. G. Jonsson, "Partially transparent Jaumann-like absorber applied to a curved structure," *Int. J. Antennas Propag*., vol. 2011, 2011.
[19] A. Motevasselian and B. L. G. Jonsson, "Design of a wideband rasorber with a polarization-sensitive transparent window," *IET Microw. Antennas Propag*., vol. 6, no. 7, pp. 747-755, 2012.
[20] A. Ito, H. Ebara, H. Nakajima, K. Wada and O. Hashimoto, "An experimental study of a λ/4 wave absorber using a frequency-selective surface," *Microw. Opt. Tech. Lett*., vol. 28, no. 5, pp. 321-323, Mar. 2001.
[21] C. Mias, "Frequency selective absorption using lumped element frequency selective surfaces," *Electron. Lett*., vol. 39, no. 11, pp. 847-849, May 2003.
[22] D. M. Pozar, *Microwave Engineering*, 4th ed. NJ: John Wiley & Sons, Inc., 2012.
[23] R. J. Langley and E. A. Parker, "Equivalent circuit model for arrays of square loops," *Electron. Lett*., vol. 18, no. 7, pp. 294-296, Apr. 1982.
[24] E. A. Parker, "The gentleman's guide to frequency selective surfaces," presented at 17th Q.M.W. Antenna Symp. London, Apr. 1991.
[25] B. Li and Z. Shen, "Synthesis of quasi-elliptic bandpass frequency-selective surface using cascaded loop arrays," *IEEE Trans. Antennas Propag*., vol. 61, no. 6, pp. 3053-3059, Jun. 2013.
[26] B. A. Munk, P. Munk and J. Pryor, "On designing Jaumann and circuit analog absorber (CA absorbers) for oblique angle of incidence," *IEEE Trans. Antennas Propag*., vol. 55, no. 1, pp. 186-193, Jan. 2007.
[27] Y. Shang, Z. Shen and S. Xiao, "On the design of single-layer circuit analog absorber using double-square-loop array," *IEEE Trans. Antennas Propag*., vol. 61, no. 12, pp. 6022-6029, Dec. 2013.

Yuping Shang received the B.S. degree in electronic information science and technology from the Sichuan University of Science and Engineering, Zigong, China, in 2009, and is currently pursuing the Ph.D. degree in radio physics at the University of Electronic Science and Technology of China, Chengdu, China.

His research interests include design of radar absorber, antenna and array.

Zhongxiang Shen (M'98-SM'04) received the B. Eng. degree from the University of Electronic Science and Technology of China, Chengdu, China, in 1987, the M. S. degree from Southeast University, Nanjing, China, in 1990, and the PhD degree from the University of Waterloo, Waterloo, Ontario, Canada, in 1997, all in electrical engineering.

From 1990 to 1994, he was with Nanjing University of Aeronautics and Astronautics, China. He was with Com Dev Ltd., Cambridge, Canada, as an Advanced Member of Technical Staff in 1997. He spent six months each in 1998, first with the Gordon McKay Laboratory, Harvard University, Cambridge, MA, and then with the Radiation Laboratory, the University of Michigan, Ann Arbor, MI, as a Postdoctoral Fellow. In 1999, he joined Nanyang Technological University (NTU), Singapore, as an assistant professor. He has been an associate professor in the School of Electrical and Electronic Engineering, NTU, since Jan. 2004.

Dr. Shen is a member of the Antennas and Propagation and Microwave Theory and Techniques Societies of the IEEE. He served as Chair of the IEEE MTT/AP Singapore Chapter. He currently serves as the Chair of AP-S Chapter Activities Committee.

His research interests include design of small and planar antennas for various wireless communication systems, analysis and design of frequency-selective structures, hybrid numerical techniques for modeling RF/microwave

components and antennas. He has authored or co-authored more than 110 journal papers and another 100 conference papers.

Shaoqiu Xiao (M'05) received the Ph.D. degree in Electromagnetic field and microwave engineering from the University of Electronic Science and Technology of China (UESTC), Chengdu, China, in 2003. From January 2004 to June 2004, he joined UESTC as an assistant professor. From July 2004 to March 2006, he worked for the Wireless Communications Laboratory, National Institute of Information and Communications Technology of Japan (NICT), Singapore, as a researcher with the focus on the planar antenna and smart antenna design and optimization. From July 2006 to June 2010, he worked for UESTC as an associate professor and now he is working for UESTC as a professor.

His current research interests include planar antenna and array, microwave passive circuits and electromagnetic in ultrawide band communication. He has authored/coauthored more than 120 technical journals, conference papers, books and book chapters.